University of Texas Rio Grande Valley

ScholarWorks @ UTRGV

Physics and Astronomy Faculty Publications and Presentations

College of Sciences

2009

First LIGO search for gravitational wave bursts from cosmic (super)strings

Matthew Benacquista
The University of Texas Rio Grande Valley

Teviet Creighton
The University of Texas Rio Grande Valley

Mario C. Diaz
The University of Texas Rio Grande Valley

R. Grosso

K. Hayama

See next page for additional authors

Follow this and additional works at: https://scholarworks.utrgv.edu/pa_fac

🇨 Part of the Astrophysics and Astronomy Commons, and the Physics Commons

Authors

Matthew Benacquista, Teviet Creighton, Mario C. Diaz, R. Grosso, K. Hayama, H. Lei, Soumya Mohanty, Soma Mukherjee, M. Rakhmanov, Joseph D. Romano, Robert Stone, and Lappoon R. Tang

First LIGO search for gravitational wave bursts from cosmic (super)strings

B. P. Abbott,[17] R. Abbott,[17] R. Adhikari,[17] P. Ajith,[2] B. Allen,[2,60] G. Allen,[35] R. S. Amin,[21] S. B. Anderson,[17]
W. G. Anderson,[60] M. A. Arain,[47] M. Araya,[17] H. Armandula,[17] P. Armor,[60] Y. Aso,[17] S. Aston,[46] P. Aufmuth,[16]
C. Aulbert,[2] S. Babak,[1] P. Baker,[24] S. Ballmer,[17] C. Barker,[18] D. Barker,[18] B. Barr,[48] P. Barriga,[59] L. Barsotti,[20]
M. A. Barton,[17] I. Bartos,[10] R. Bassiri,[48] M. Bastarrika,[48] B. Behnke,[1] M. Benacquista,[42] J. Betzwieser,[17]
P. T. Beyersdorf,[31] I. A. Bilenko,[25] G. Billingsley,[17] R. Biswas,[60] E. Black,[17] J. K. Blackburn,[17] L. Blackburn,[20] D. Blair,[59]
B. Bland,[18] T. P. Bodiya,[20] L. Bogue,[19] R. Bork,[17] V. Boschi,[17] S. Bose,[61] P. R. Brady,[60] V. B. Braginsky,[25] J. E. Brau,[53]
D. O. Bridges,[19] M. Brinkmann,[2] A. F. Brooks,[17] D. A. Brown,[36] A. Brummit,[30] G. Brunet,[20] A. Bullington,[35]
A. Buonanno,[49] O. Burmeister,[2] R. L. Byer,[35] L. Cadonati,[50] J. B. Camp,[26] J. Cannizzo,[26] K. C. Cannon,[17] J. Cao,[20]
L. Cardenas,[17] S. Caride,[51] G. Castaldi,[56] S. Caudill,[21] M. Cavaglià,[39] C. Cepeda,[17] T. Chalermsongsak,[17] E. Chalkley,[48]
P. Charlton,[9] S. Chatterji,[17] S. Chelkowski,[46] Y. Chen,[1,6] N. Christensen,[8] C. T. Y. Chung,[38] D. Clark,[35] J. Clark,[7]
J. H. Clayton,[60] T. Cokelaer,[7] C. N. Colacino,[12] R. Conte,[55] D. Cook,[18] T. R. C. Corbitt,[20] N. Cornish,[24] D. Coward,[59]
D. C. Coyne,[17] J. D. E. Creighton,[60] T. D. Creighton,[42] A. M. Cruise,[46] R. M. Culter,[46] A. Cumming,[48] L. Cunningham,[48]
S. L. Danilishin,[25] K. Danzmann,[2,16] B. Daudert,[17] G. Davies,[7] E. J. Daw,[40] D. DeBra,[35] J. Degallaix,[2] V. Dergachev,[51]
S. Desai,[37] R. DeSalvo,[17] S. Dhurandhar,[15] M. Díaz,[42] A. Dietz,[7] F. Donovan,[20] K. L. Dooley,[47] E. E. Doomes,[34]
R. W. P. Drever,[5] J. Dueck,[2] I. Duke,[20] J.-C. Dumas,[59] J. G. Dwyer,[10] C. Echols,[17] M. Edgar,[48] A. Effler,[18] P. Ehrens,[17]
E. Espinoza,[17] T. Etzel,[17] M. Evans,[20] T. Evans,[19] S. Fairhurst,[7] Y. Faltas,[47] Y. Fan,[59] D. Fazi,[17] H. Fehrmann,[2] L. S. Finn,[37]
K. Flasch,[60] S. Foley,[20] C. Forrest,[54] N. Fotopoulos,[60] A. Franzen,[16] M. Frede,[2] M. Frei,[41] Z. Frei,[12] A. Freise,[46] R. Frey,[53]
T. Fricke,[19] P. Fritschel,[20] V. V. Frolov,[19] M. Fyffe,[19] V. Galdi,[56] J. A. Garofoli,[36] I. Gholami,[1] J. A. Giaime,[21,19]
S. Giampanis,[2] K. D. Giardina,[19] K. Goda,[20] E. Goetz,[51] L. M. Goggin,[60] G. González,[21] M. L. Gorodetsky,[25] S. Goßler,[2]
R. Gouaty,[21] A. Grant,[48] S. Gras,[59] C. Gray,[18] M. Gray,[4] R. J. S. Greenhalgh,[30] A. M. Gretarsson,[11] F. Grimaldi,[20]
R. Grosso,[42] H. Grote,[2] S. Grunewald,[1] M. Guenther,[18] E. K. Gustafson,[17] R. Gustafson,[51] B. Hage,[16] J. M. Hallam,[46]
D. Hammer,[60] G. D. Hammond,[48] C. Hanna,[17] J. Hanson,[19] J. Harms,[52] G. M. Harry,[20] I. W. Harry,[7] E. D. Harstad,[53]
K. Haughian,[48] K. Hayama,[42] J. Heefner,[17] I. S. Heng,[48] A. Heptonstall,[17] M. Hewitson,[2] S. Hild,[46] E. Hirose,[36] D. Hoak,[19]
K. A. Hodge,[17] K. Holt,[19] D. J. Hosken,[45] J. Hough,[48] D. Hoyland,[59] B. Hughey,[20] S. H. Huttner,[48] D. R. Ingram,[18]
T. Isogai,[8] M. Ito,[53] A. Ivanov,[17] B. Johnson,[18] W. W. Johnson,[21] D. I. Jones,[57] G. Jones,[7] R. Jones,[48] L. Ju,[59] P. Kalmus,[17]
V. Kalogera,[28] S. Kandhasamy,[52] J. Kanner,[49] D. Kasprzyk,[46] E. Katsavounidis,[20] K. Kawabe,[18] S. Kawamura,[27]
F. Kawazoe,[2] W. Kells,[17] D. G. Keppel,[17] A. Khalaidovski,[2] F. Y. Khalili,[25] R. Khan,[10] E. Khazanov,[14] P. King,[17]
J. S. Kissel,[21] S. Klimenko,[47] K. Kokeyama,[27] V. Kondrashov,[17] R. Kopparapu,[37] S. Koranda,[60] D. Kozak,[17] B. Krishnan,[1]
R. Kumar,[48] P. Kwee,[16] P. K. Lam,[4] M. Landry,[18] B. Lantz,[35] A. Lazzarini,[17] H. Lei,[42] M. Lei,[17] N. Leindecker,[35]
I. Leonor,[53] C. Li,[6] H. Lin,[47] P. E. Lindquist,[17] T. B. Littenberg,[24] N. A. Lockerbie,[58] D. Lodhia,[46] M. Longo,[56]
M. Lormand,[19] P. Lu,[35] M. Lubinski,[18] A. Lucianetti,[47] H. Lück,[2,16] B. Machenschalk,[1] M. MacInnis,[20] M. Mageswaran,[17]
K. Mailand,[17] I. Mandel,[28] V. Mandic,[52] S. Márka,[10] Z. Márka,[10] A. Markosyan,[35] J. Markowitz,[20] E. Maros,[17]
I. W. Martin,[48] R. M. Martin,[47] J. N. Marx,[17] K. Mason,[20] F. Matichard,[21] L. Matone,[10] R. A. Matzner,[41] N. Mavalvala,[20]
R. McCarthy,[18] D. E. McClelland,[4] S. C. McGuire,[34] M. McHugh,[23] G. McIntyre,[17] D. J. A. McKechan,[7] K. McKenzie,[4]
M. Mehmet,[2] A. Melatos,[38] A. C. Melissinos,[54] D. F. Menéndez,[37] G. Mendell,[18] R. A. Mercer,[60] S. Meshkov,[17]
C. Messenger,[2] M. S. Meyer,[19] J. Miller,[48] J. Minelli,[37] Y. Mino,[6] V. P. Mitrofanov,[25] G. Mitselmakher,[47] R. Mittleman,[20]
O. Miyakawa,[17] B. Moe,[60] S. D. Mohanty,[42] S. R. P. Mohapatra,[50] G. Moreno,[18] T. Morioka,[27] K. Mors,[2] K. Mossavi,[2]
C. MowLowry,[4] G. Mueller,[47] H. Müller-Ebhardt,[2] D. Muhammad,[19] S. Mukherjee,[42] H. Mukhopadhyay,[15] A. Mullavey,[4]
J. Munch,[45] P. G. Murray,[48] E. Myers,[18] J. Myers,[18] T. Nash,[17] J. Nelson,[48] G. Newton,[48] A. Nishizawa,[27] K. Numata,[26]
J. O'Dell,[30] B. O'Reilly,[19] R. O'Shaughnessy,[37] E. Ochsner,[49] G. H. Ogin,[17] D. J. Ottaway,[45] R. S. Ottens,[47] H. Overmier,[19]
B. J. Owen,[37] Y. Pan,[49] C. Pankow,[47] M. A. Papa,[1,60] V. Parameshwaraiah,[18] P. Patel,[17] M. Pedraza,[17] S. Penn,[13]
A. Perreca,[46] V. Pierro,[56] I. M. Pinto,[56] M. Pitkin,[48] H. J. Pletsch,[2] M. V. Plissi,[48] F. Postiglione,[55] M. Principe,[56] R. Prix,[2]
L. Prokhorov,[25] O. Punken,[2] V. Quetschke,[47] F. J. Raab,[18] D. S. Rabeling,[4] H. Radkins,[18] P. Raffai,[12] Z. Raics,[10] N. Rainer,[2]
M. Rakhmanov,[42] V. Raymond,[28] C. M. Reed,[18] T. Reed,[22] H. Rehbein,[2] S. Reid,[48] D. H. Reitze,[47] R. Riesen,[19] K. Riles,[51]
B. Rivera,[18] P. Roberts,[3] N. A. Robertson,[17,48] C. Robinson,[7] E. L. Robinson,[1] S. Roddy,[19] C. Röver,[2] J. Rollins,[10]
J. D. Romano,[42] J. H. Romie,[19] S. Rowan,[48] A. Rüdiger,[2] P. Russell,[17] K. Ryan,[18] S. Sakata,[27] L. Sancho de la Jordana,[44]
V. Sandberg,[18] V. Sannibale,[17] L. Santamaría,[1] S. Saraf,[32] P. Sarin,[20] B. S. Sathyaprakash,[7] S. Sato,[27] M. Satterthwaite,[4]
P. R. Saulson,[36] R. Savage,[18] P. Savov,[6] M. Scanlan,[22] R. Schilling,[2] R. Schnabel,[2] R. Schofield,[53] B. Schulz,[2]
B. F. Schutz,[1,7] P. Schwinberg,[18] J. Scott,[48] S. M. Scott,[4] A. C. Searle,[17] B. Sears,[17] F. Seifert,[2] D. Sellers,[19]

A. S. Sengupta,[17] A. Sergeev,[14] B. Shapiro,[20] P. Shawhan,[49] D. H. Shoemaker,[20] A. Sibley,[19] X. Siemens,[60] D. Sigg,[18] S. Sinha,[35] A. M. Sintes,[44] B. J. J. Slagmolen,[4] J. Slutsky,[21] J. R. Smith,[36] M. R. Smith,[17] N. D. Smith,[20] K. Somiya,[6] B. Sorazu,[48] A. Stein,[20] L. C. Stein,[20] S. Steplewski,[61] A. Stochino,[17] R. Stone,[42] K. A. Strain,[48] S. Strigin,[25] A. Stroeer,[26] A. L. Stuver,[19] T. Z. Summerscales,[3] K.-X. Sun,[35] M. Sung,[21] P. J. Sutton,[7] G. P. Szokoly,[12] D. Talukder,[61] L. Tang,[42] D. B. Tanner,[47] S. P. Tarabrin,[25] J. R. Taylor,[2] R. Taylor,[17] J. Thacker,[19] K. A. Thorne,[19] K. S. Thorne,[6] A. Thüring,[16] K. V. Tokmakov,[48] C. Torres,[19] C. Torrie,[17] G. Traylor,[19] M. Trias,[44] D. Ugolini,[43] J. Ulmen,[35] K. Urbanek,[35] H. Vahlbruch,[16] M. Vallisneri,[6] C. Van Den Broeck,[7] M. V. van der Sluys,[28] A. A. van Veggel,[48] S. Vass,[17] R. Vaulin,[60] A. Vecchio,[46] J. Veitch,[46] P. Veitch,[45] C. Veltkamp,[2] A. Villar,[17] C. Vorvick,[18] S. P. Vyachanin,[25] S. J. Waldman,[20] L. Wallace,[17] R. L. Ward,[17] A. Weidner,[2] M. Weinert,[2] A. J. Weinstein,[17] R. Weiss,[20] L. Wen,[6,59] S. Wen,[21] K. Wette,[4] J. T. Whelan,[1,29] S. E. Whitcomb,[17] B. F. Whiting,[47] C. Wilkinson,[18] P. A. Willems,[17] H. R. Williams,[37] L. Williams,[47] B. Willke,[2,16] I. Wilmut,[30] L. Winkelmann,[2] W. Winkler,[2] C. C. Wipf,[20] A. G. Wiseman,[60] G. Woan,[48] R. Wooley,[19] J. Worden,[18] W. Wu,[47] I. Yakushin,[19] H. Yamamoto,[17] Z. Yan,[59] S. Yoshida,[33] M. Zanolin,[11] J. Zhang,[51] L. Zhang,[17] C. Zhao,[59] N. Zotov,[22] M. E. Zucker,[20] H. zur Mühlen,[16] J. Zweizig,[17] and F. Robinet[62]

(The LIGO Scientific Collaboration)[*]

[1]*Albert-Einstein-Institut, Max-Planck-Institut für Gravitationsphysik, D-14476 Golm, Germany*
[2]*Albert-Einstein-Institut, Max-Planck-Institut für Gravitationsphysik, D-30167 Hannover, Germany*
[3]*Andrews University, Berrien Springs, Michigan 49104 USA*
[4]*Australian National University, Canberra, 0200, Australia*
[5]*California Institute of Technology, Pasadena, California 91125, USA*
[6]*Caltech-CaRT, Pasadena, California 91125, USA*
[7]*Cardiff University, Cardiff, CF24 3AA, United Kingdom*
[8]*Carleton College, Northfield, Minnesota 55057, USA*
[9]*Charles Sturt University, Wagga Wagga, NSW 2678, Australia*
[10]*Columbia University, New York, New York 10027, USA*
[11]*Embry-Riddle Aeronautical University, Prescott, Arizona 86301 USA*
[12]*Eötvös University, ELTE 1053 Budapest, Hungary*
[13]*Hobart and William Smith Colleges, Geneva, New York 14456, USA*
[14]*Institute of Applied Physics, Nizhny Novgorod, 603950, Russia*
[15]*Inter-University Center for Astronomy and Astrophysics, Pune-411007, India*
[16]*Leibniz Universität Hannover, D-30167 Hannover, Germany*
[17]*LIGO-California Institute of Technology, Pasadena, California 91125, USA*
[18]*LIGO-Hanford Observatory, Richland, Washington 99352, USA*
[19]*LIGO-Livingston Observatory, Livingston, Louisiana 70754, USA*
[20]*LIGO-Massachusetts Institute of Technology, Cambridge, Massachusetts 02139, USA*
[21]*Louisiana State University, Baton Rouge, Louisiana 70803, USA*
[22]*Louisiana Tech University, Ruston, Louisiana 71272, USA*
[23]*Loyola University, New Orleans, Louisiana 70118, USA*
[24]*Montana State University, Bozeman, Montana 59717, USA*
[25]*Moscow State University, Moscow, 119992, Russia*
[26]*NASA/Goddard Space Flight Center, Greenbelt, Maryland 20771, USA*
[27]*National Astronomical Observatory of Japan, Tokyo 181-8588, Japan*
[28]*Northwestern University, Evanston, Illinois 60208, USA*
[29]*Rochester Institute of Technology, Rochester, New York 14623, USA*
[30]*Rutherford Appleton Laboratory, Harwell Science and Innovation Campus, Chilton, Didcot, Oxon OX11 0QX United Kingdom*
[31]*San Jose State University, San Jose, California 95192, USA*
[32]*Sonoma State University, Rohnert Park, California 94928, USA*
[33]*Southeastern Louisiana University, Hammond, Louisiana 70402, USA*
[34]*Southern University and A&M College, Baton Rouge, Louisiana 70813, USA*
[35]*Stanford University, Stanford, California 94305, USA*
[36]*Syracuse University, Syracuse, New York 13244, USA*
[37]*The Pennsylvania State University, University Park, Pennsylvania 16802, USA*
[38]*The University of Melbourne, Parkville VIC 3010, Australia*
[39]*The University of Mississippi, University, Mississippi 38677, USA*
[40]*The University of Sheffield, Sheffield S10 2TN, United Kingdom, USA*
[41]*The University of Texas at Austin, Austin, Texas 78712, USA*
[42]*The University of Texas at Brownsville and Texas Southmost College, Brownsville, Texas 78520, USA*

[43]*Trinity University, San Antonio, Texas 78212, USA*
[44]*Universitat de les Illes Balears, E-07122 Palma de Mallorca, Spain*
[45]*University of Adelaide, Adelaide, SA 5005, Australia*
[46]*University of Birmingham, Birmingham, B15 2TT, United Kingdom*
[47]*University of Florida, Gainesville, Florida 32611, USA*
[48]*University of Glasgow, Glasgow, G12 8QQ, United Kingdom*
[49]*University of Maryland, College Park, Maryland 20742 USA*
[50]*University of Massachusetts-Amherst, Amherst, Massachusetts 01003, USA*
[51]*University of Michigan, Ann Arbor, Michigan 48109, USA*
[52]*University of Minnesota, Minneapolis, Minnesota 55455, USA*
[53]*University of Oregon, Eugene, Oregon 97403, USA*
[54]*University of Rochester, Rochester, New York 14627, USA*
[55]*University of Salerno, 84084 Fisciano (Salerno), Italy*
[56]*University of Sannio at Benevento, I-82100 Benevento, Italy*
[57]*University of Southampton, Southampton, SO17 1BJ, United Kingdom*
[58]*University of Strathclyde, Glasgow, G1 1XQ, United Kingdom*
[59]*University of Western Australia, Crawley, Washington 6009, Australia, USA*
[60]*University of Wisconsin-Milwaukee, Milwaukee, Wisconsin 53201, USA*
[61]*Washington State University, Pullman, Washington 99164, USA*
[62]*Laboratoire de l'Accélérateur Linéaire, Univ Paris-Sud, CNRS/IN2P3, Orsay, France*

We report on a matched-filter search for gravitational wave bursts from cosmic string cusps using LIGO data from the fourth science run (S4) which took place in February and March 2005. No gravitational waves were detected in 14.9 days of data from times when all three LIGO detectors were operating. We interpret the result in terms of a frequentist upper limit on the rate of gravitational wave bursts and use the limits on the rate to constrain the parameter space (string tension, reconnection probability, and loop sizes) of cosmic string models. Many grand unified theory-scale models (with string tension $G\mu/c^2 \approx 10^{-6}$) can be ruled out at 90% confidence for reconnection probabilities $p \leq 10^{-3}$ if loop sizes are set by gravitational back reaction.

I. INTRODUCTION

Cosmic strings are one-dimensional topological defects that can form during phase transitions in the early universe [1,2]. Topological defect formation is generic in grand unified theories (GUTs), and cosmic string production specifically is generic in supersymmetric GUTs [3]. In string theory motivated cosmological models, cosmic strings may also form (and are referred to as cosmic superstrings to differentiate them from strings formed in phase transitions) [4–13]. There are important differences between cosmic superstrings and field theoretic strings. When superstrings meet they reconnect with probability p that can be less than unity. This is partly due to the fact that fundamental strings interact probabilistically. Furthermore, these models have extra spatial dimensions so that even though two strings may meet in 3 dimensions, they miss each other in the extra dimensions. These two effects result in values of p in the range 10^{-3}–1 [9]. In addition, in string theory motivated cosmological models, more than one type of string may form.

Cosmic strings and superstrings may produce a variety of astrophysical signatures including gamma ray bursts [14], ultrahigh energy cosmic rays [15], magnetogenesis [16], microlensing, strong and weak lensing [17–21], radio bursts [22], effects on the cosmic 21 cm power spectrum [23], effects on the cosmic microwave background (CMB) at small angular scales [24,25], and effects on the CMB polarization [26].

Cosmic strings and superstrings can also produce powerful bursts of gravitational waves [27–31]. The most potent bursts are produced at regions of string called cusps which acquire large Lorentz boosts. The formation of cusps on cosmic strings is generic, and cusp gravitational waveforms are simple and robust [32,33]. The large mass per unit length of cosmic strings combined with the large Lorentz boost may result in signals detectable by Earth-based interferometric gravitational wave detectors such as LIGO [34] and Virgo [35]. Thus, gravitational waves may provide a powerful probe of early universe physics.

The LIGO detector network is comprised of three laser interferometers. Two of them are located at the Hanford, WA site: a four-kilometer arm instrument referred to as H1, and a two-kilometer arm instrument referred to as H2. A second four-kilometer interferometer located at the Livingston, LA site, is referred to as L1. LIGO's fourth science run (S4) took place between February 22, 2005 and March 23, 2005. The configuration of the LIGO instru-

*http://www.ligo.org

ments during the fourth science run (S4) is described in [36]. The sensitivity of this run was significantly better than that of previous runs: at the low frequencies relevant to this search, close to a factor of 10 more sensitive than the previous science run S3, though still about a factor of 2 less sensitive than LIGO's most recent science run (S5), which was at design sensitivity.

In this work, we report on the results of a matched-filter search for bursts from cosmic string cusps performed on 14.9 days of S4 data. We implement the data analysis methods described in [31] using a simple triple coincidence scheme. No gravitational waves were detected, and we interpret the result in terms of a frequentist upper limit on the rate using the loudest event technique [37]. We use the upper limit on the rate to constrain the parameter space of cosmic strings models. The sensitivity of the LIGO instruments during the S4 run does not allow us to place constraints as tight as the indirect bounds from big bang nucleosynthesis [38]. In the future, however, we expect our sensitivity to surpass these limits for large areas of cosmic string model parameter space.

In Sec. II we discuss data selection, data analysis techniques, and describe the analysis pipeline. In Sec. III we describe the computation of the rate of accidental events we expect to survive the thresholds and consistency checks of the pipeline (the so-called background), and we compare it to the events that made it to the end of the pipeline in our search (the so-called foreground). In Sec. IV we show how we estimate the sensitivity of the analysis using simulated gravitational wave signals. We compute the efficiency of our pipeline, the fraction of simulated signals that we detect, as a function of the strength of the signals. In Sec. V we show how to estimate the rate of burst events we expect, the effective rate, using the efficiency curves and the cosmological rate of events. We show the constraints our data place on the parameter space of cosmic string models. We conclude in Sec. VI.

II. DATA ANALYSIS

A. Data selection and conditioning

All available S4 science data when all three instruments were operating (triple coincident data) were used except for periods
  (1) with overflows in the error signal digitizer,
  (2) when airplanes flew over the detector sites,
  (3) thirty seconds prior to loss of lock (loss of resonance of the Fabry-Perot cavities in the arms) of any instrument,
  (4) of excessive wind,
  (5) of excessive seismic activity, and
  (6) with calibration uncertainties larger than 10%.
The total time of triple coincident data available after these cuts is 14.9 days. Calibration of the data used in this analysis was performed in the time domain [39]. The data were high-pass filtered near 30 Hz to remove unnec-

essary low frequency content and down-sampled from the original LIGO sampling rate of 16384 to 4096 Hz.

B. Matched filters and templates

For each of the three LIGO instruments, we then performed a matched-filter search on this data for gravitational bursts from cosmic string cusps, i.e. linearly polarized signals of the form [28]

$$h_+(f) = Bf^{-4/3}\Theta(f_h - f)\Theta(f - f_l). \tag{1}$$

The amplitude of the cusp waveform is $B \sim G\mu L^{2/3}/(c^3 r)$, where G is Newton's constant, μ is the mass per unit length of the string, L is the size of the feature on the string that produces the cusp, and r is the distance between the cusp and the point of observation. In natural units $G\mu/c^2$ can be thought of as the dimensionless mass per unit length, or tension, of cosmic strings. For GUT-scale cosmic strings, for example, $G\mu/c^2 = 10^{-6}$ [2]. The size L of the feature on the string that produces the cusp also determines the low frequency cutoff f_l. Since L is expected to be cosmological, for example, the size of a cosmic string loop, the low frequency cutoff of *detectable* radiation is determined by the low frequency behavior of the instruments: for the LIGO instruments by seismic noise. The high frequency cutoff depends on the angle θ between the line of sight and the direction of the cusp. It is given by $f_h \sim 2c/(\theta^3 L)$ and can be arbitrarily large (up to the inverse of the light crossing time of the width of strings).

Following [31] for our templates, we take

$$\tau(f) = f^{-4/3}\Theta(f_h - f)\Theta(f - f_l), \tag{2}$$

so that $h(f) = A\tau(f)$. We can normalize our templates by defining the detector-noise-weighted inner product [40] in terms of the two frequency series $x(f)$ and $y(f)$ as

$$(x|y) \equiv 4\Re \int_0^\infty df \frac{x(f)y^*(f)}{S_h(f)}. \tag{3}$$

Here, $S_h(f)$ is the single-sided spectral density defined by $\langle n(f)n^*(f')\rangle = \frac{1}{2}\delta(f - f')S_h(f)$, and $n(f)$ is the Fourier transform of the detector noise. We take the inner product of a template with itself to be $\sigma^2 = (\tau|\tau)$ and define the normalized template $\hat{\tau} \equiv \tau/\sigma$, so that $(\hat{\tau}|\hat{\tau}) = 1$.

The calibrated output of an interferometer can be written as

$$s(t) = n(t) + h(t), \tag{4}$$

where $n(t)$ is the instrumental noise, and $h(t) = F_+ h_+(t)$ the gravitational wave signal. The antenna pattern response function to $+$-polarized gravitational waves, F_+ is a function of the sky location of the cusp and the polarization angle. The signal to noise ratio (SNR) is defined in terms of the inner product as $\rho \equiv (s|\hat{\tau})$. For the case of Gaussian noise and in the absence of a signal, the SNR is a Gaussian

variable with zero mean and unit variance. In the presence of a signal of amplitude A, the signal to noise ratio is a Gaussian random variable, with mean $A\sigma$ and unit variance. Since the average SNR is $\langle \rho \rangle = A\sigma$, for a particular realization of the measured SNR ρ, we can identify a signal amplitude

$$A = \rho/\sigma, \tag{5}$$

which has an average value $\langle A \rangle = F_+ B$.

In our search, we set $f_l = 50$ Hz to be our low frequency cutoff. Because of the low frequency behavior of our instruments, a negligible SNR would be gained by including frequencies lower than 50 Hz. We look for signals with high frequency cutoffs f_h in the range 75–2048 Hz. The sensitivity of the instruments is such that very little is lost by limiting the search to signals with high frequency cutoffs above 75 Hz and below 2048 Hz. The only template parameter is the high frequency cutoff f_h and the template bank (the set of templates that determines the signals we search for) is constructed iteratively by computing the overlap between adjacent templates [31]. The maximum fractional loss of signal to noise is set to 0.05 and along with the spectrum, determines the spacing between the high frequency cutoffs of the different templates. The spectrum $S_h(f)$ is estimated using the median-mean method [41] which is fairly robust against nonstationarities in the data, including loud simulated signal injections.

C. Trigger generation

To produce our trigger data, we proceed as follows. We apply the matched filter for each template and all possible arrival times using fast Fourier transform convolution (as described in [31]). This procedure results in a time series for the SNR sampled at 4096 Hz for every template. In each of these time series, we search for clusters of values above the threshold $\rho_{\text{th}} = 4$ which we identify as triggers. For each trigger we determine

   (a) the SNR ρ of the trigger (the maximum SNR of the cluster),
   (b) the peak time of the trigger (the location in time of the trigger SNR),
   (c) the start time of the trigger (the first value above threshold in the cluster),
   (d) the duration of the trigger (the length of the cluster),
   (e) the high frequency cutoff of the template, and
   (f) the amplitude of the trigger A, given by $A = \rho/\sigma$, where σ is the template normalization.

When several templates result in triggers that occur within a time of 0.1 s, we select the trigger with the largest SNR within that time window.

We apply this procedure to the data sets of the three LIGO interferometers to produce a list of triggers for each instrument.

D. Trigger consistency checks

To reduce the rate of events unassociated with gravitational waves (noise induced events), we demand that the peak times of triggers in each instrument be coincident in time with triggers in the other two instruments. The time window used for H1-H2 events is 2 ms. This coincidence window allows for calibration uncertainties as well as shifts in the peak times of triggers induced by fluctuations in the noise. For coincidence between events in either of the two Hanford instruments with events in the Livingston interferometer, a 12 ms coincidence window is used. This allows for the maximum light travel time between sites of 10 ms along with calibration uncertainties and shifting of the peak location due to noise. We require strict triple coincidence: in order for an event in one interferometer to survive, it must be coincident with events in the other two instruments and those two events must also be coincident.

Additionally, we impose a symmetric consistency check on the amplitudes of H1 and H2 coincident events [31]. In particular, for H1 events we demand that

$$\frac{|A_{\text{H1}} - A_{\text{H2}}|}{A_{\text{H1}}} < \left(\frac{\delta}{\rho_{\text{H1}}} + \kappa\right), \tag{6}$$

along with an analogous requirement for H2 events. Here, δ is the number of standard deviations of amplitude difference we allow, and κ is an additional fractional difference that accounts for other sources of uncertainty such as the calibration. We conservatively set $\delta = 3$ and $\kappa = 0.5$. The purpose of this loose cut on the amplitude of events is to eliminate large SNR events seen in one instrument but not in the other. These events are not due to gravitational waves but rather to instrumental glitches in the data streams. It is worth pointing out that because each instrument has its own antenna response factor F_+ that depends on the orientation and direction of the gravitational wave, the H1-H2 amplitude consistency test cannot be applied to H1-L1 or H2-L1. Instruments that are not colocated may have different values of F_+, and therefore the measured amplitudes A could differ significantly.

Both time coincidence and amplitude consistency checks reduce the rate of events in each instrument from about 1 Hz to about 10 μHz. To simplify the analysis in the following, we only use the results and statistics for the H1 events.

III. FOREGROUND AND BACKGROUND

To estimate the rate of accidental coincidences that survive our consistency checks, the so-called background, we time shift the trigger sets relative to one another and look for coincident events. We do not perform time shifts on the two Hanford trigger sets. Environmental disturbances are known to cause correlations between triggers in both interferometers, and the effect of time shifting the two
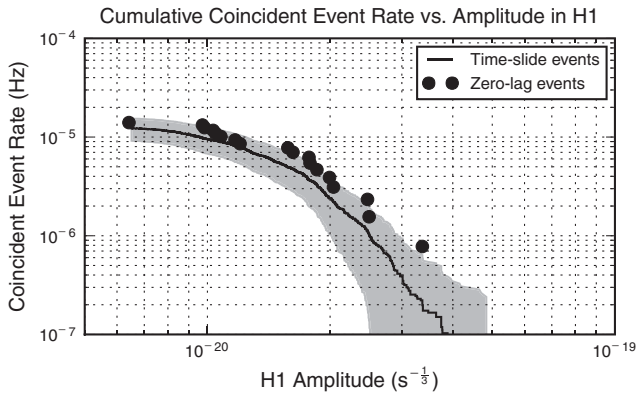
FIG. 1.　Plot of the cumulative rate of events as a function of the amplitude for both foreground events (filled circles), as well as average number of events found in the time shifted data (stair steps). The shaded region corresponds to 1-σ variations measured in the time shifts.

Hanford trigger sets would be to underestimate the background. We therefore take the double coincident H1 and H2 triggers (which already satisfy the amplitude consistency check) and time shift them relative to the L1 trigger set. This amounts to treating the two Hanford instruments as a single trigger generator, on the same footing as L1 but with a much smaller trigger rate. For each trigger in each time shift, we then demand the first consistency criterion be satisfied, namely, that each Hanford trigger peak be within 12 ms of a Livingston trigger peak. We performed 100 time shifts, with Livingston triggers shifted by approximately 1.79 s, the total time shift ranging from -89.3 s to 89.3 s. The time shifts are large enough that coincident events cannot result from gravitational wave bursts from cosmic string cusps.

Figure 1 summarizes the results of this procedure for the H1 trigger set. We plot the cumulative rate of events for both foreground (unshifted) events (filled circles), as well as the average rate of events found in the time shifted data (stair steps) binned in amplitude. The shaded region corresponds to 1-σ uncertainties computed from the variations in the number of events found in the time shifted data.

The loudest H1 event has an amplitude of $A^L = 3.4 \times 10^{-20}$ s$^{-1/3}$. There are no foreground events which deviate significantly from the time slides, and a Kolmogorov-Smirnov test confirms that the foreground and background distributions are consistent at the 77% confidence level. We therefore conclude that no gravitational waves have been detected in this search.

IV. EFFICIENCY

To determine our sensitivity and construct an upper limit, we injected over 7400 simulated cusp signals into our data set and performed a search identical to the one described above.

The distribution of high frequency cutoffs f_h for the injected signals is $dN \propto f_h^{-5/3} df_h$, appropriate for the cusp signals we are seeking [31]. The lowest high frequency cutoff injected is $f_* = 75$ Hz, coinciding with the lowest high frequency cutoff of our templates. The amplitudes are distributed logarithmically between $B = 6 \times 10^{-21}$ s$^{-1/3}$ and $B = 10^{-17}$ s$^{-1/3}$ spanning the range of detectability. The sources are placed isotropically in the sky with sufficient separation in time so as not to unduly bias the spectrum estimate needed to perform the matched filter.

An injection is found if its peak time lies between the start time and the end time of an H1 triple coincident trigger. We record the recovered amplitude of the injection, which is different (typically smaller) than the injected amplitude because of antenna pattern effects as well as noise induced fluctuations.

The result of our injection run is summarized in Fig. 2. We plot the efficiency $\epsilon(B)$ (the fraction of injections detected in the triple coincident H1 trigger set) as a function of the injected amplitude B for recovered H1 amplitudes A greater than our loudest event $A^L = 3.4 \times 10^{-20}$ s$^{-1/3}$ (solid line), and for *any* recovered amplitudes (dashed line). The shaded regions indicate our uncertainties in the efficiencies and amplitudes. The procedure by which these curves and their uncertainties are produced are described below in more detail.

A useful measure of our sensitivity is the injected amplitude at which we recover half of our injections. For all recovered injections, this amplitude is

$$B_{50\%} = (5.2 \pm 0.9) \times 10^{-20} \text{ s}^{-1/3}, \qquad (7)$$

and for those recovered with amplitudes above our loudest event above it is
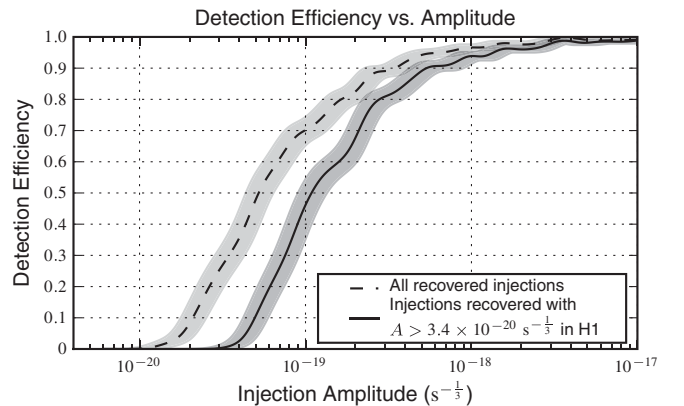

FIG. 2.　Plot of the detection efficiency $\epsilon(B)$ (fraction of events detected) as a function of the injected amplitude B. The solid curve corresponds to injections with recovered amplitudes A larger than our loudest event $A^L = 3.4 \times 10^{-20}$ s$^{-1/3}$, and the dashed curve corresponds to all recovered injections. The shaded regions indicate our uncertainty in the efficiencies and amplitudes that result from counting, binning, and calibration systematics.

$$B_{50\%}^L = (1.1 \pm 0.2) \times 10^{-19} \text{ s}^{-1/3}. \qquad (8)$$

These numbers are consistent with our expectations. In [31], a sensitivity estimate was made for initial LIGO $B_{50\%}^{\text{LIGO}} \approx 10^{-20} \text{ s}^{-1/3}$. The current search is somewhat less sensitive for two reasons. First, data from the S4 run is about a factor of 2 less sensitive than initial LIGO. Second, we demand coincidence with events in the H2 interferometer which is about a factor of 2 less sensitive than H1. Together, these account for a factor of about 4 leaving only about a 30% discrepancy between the rough initial LIGO sensitivity estimate made in [31] and Eq. (7).

As stated above, the software injections are generated randomly, with injected amplitudes that are uniformly distributed in their logarithm. Individually, each injection is either found or missed. To estimate the probability of injections with a given amplitude being recovered, we used a sliding window to count the number of software injections that were made and recovered within an interval around that amplitude. The window used was Gaussian in the logarithm of the injected amplitudes. Choosing different widths for the window will yield qualitatively equivalent but quantitatively different efficiency curves. As pointed out above, a useful measure of our sensitivity is $B_{50\%}$, and we chose the width of the Gaussian window to minimize the uncertainty in $B_{50\%}$.

Three uncertainties are associated with the efficiency curve. First, because at each point the value of the efficiency has been measured by counting a finite number of injections, there is an uncertainty in the efficiency attributable to binomial counting fluctuations. Second, there is an uncertainty in the amplitude to which a measurement of the efficiency should be assigned, on account of it having been found by counting injections spanning a range of amplitudes. Finally, uncertainties in the calibration translate into an additional uncertainty in the amplitude, on account of the injections from which the efficiency was measured having been done at amplitudes different from what was intended. The calibration uncertainty we use is 11%. This number results from the systematics in the calibration models (5%) and our use of time domain calibrated data (10%), which we combine in quadrature. The counting, amplitude range, and calibration uncertainties described above are combined in quadrature to produce the shaded regions shown in Fig. 2.

V. PARAMETER SPACE OF COSMIC STRING MODELS: CONSTRAINTS AND SENSITIVITY

For simplicity in this section, we will adopt units where the speed of light $c = 1$. The parameter space of cosmic string models we need to consider depends on whether loops in the cosmic string network are short-lived (lifetime much smaller than a Hubble time) or long-lived (lifetime much larger than a Hubble time). This, in turn, depends on loop sizes at formation. If their size is given by the gravi-

tational back reaction scale [42,43], then to a good approximation all loops have the same size at formation and they are short-lived. In this case, their size at formation at cosmic time t can be approximated by $l = \varepsilon\Gamma G\mu t$, where $\varepsilon < 1$ [30] is an unknown parameter that depends on the spectrum of perturbations on cosmic strings, and Γ is a constant related to the lifetime of loops and is measured in simulations to be $\Gamma \sim 50$. Recent cosmic string network simulations, however, suggest loops form at much larger sizes given by the network dynamics [44,45]. If this is the case, it has been shown [38] that the regions of parameter space accessible to initial LIGO are already ruled out by pulsar timing experiments. So here, we will consider only the first possibility, that loop sizes are determined by gravitational back reaction and take the size of loops at formation to be $l = \varepsilon\Gamma G\mu t$. As mentioned, unlike field theoretic cosmic strings, cosmic superstrings do not always reconnect when they meet. Rather, they reconnect with probability $p \leq 1$. The effect of the decreased reconnection probability is to increase the density of strings by a factor inversely proportional to the reconnection probability [30].

For a point in cosmic string parameter space $(G\mu, \varepsilon, p)$, we can use the efficiency curves $\epsilon(B)$ to compute the rate of bursts we expect to observe in our instruments, which we will refer to as the effective rate γ. It is given by the integral [31]

$$\gamma(G\mu, \varepsilon, p) = \int_0^\infty \epsilon(B) \frac{dR(B; G\mu, \varepsilon, p)}{dB} dB, \qquad (9)$$

where $B \sim G\mu l^{2/3}/r$ is the optimally oriented amplitude (i.e. the amplitude of events excluding antenna pattern effects), $\epsilon(B)$ is the efficiency of detecting events at an amplitude B, and $dR(B; G\mu, \varepsilon, p)$ is the cosmological rate of events with amplitude in the interval B and $B + dB$. We have taken the size of the feature that produces the cusp to be the size of the loop l.

Since we are considering loops that are small when they are formed, they are also short-lived, and at a given redshift they are all of essentially the same size. As a result, the amplitude of burst events from a given redshift is the same. In this case, rather than Eq. (9), it is easier to evaluate

$$\gamma(G\mu, \varepsilon, p) = \int_0^\infty \epsilon(z) \frac{dR(z; G\mu, \varepsilon, p)}{dz} dz. \qquad (10)$$

Here, $dR(z)$ is the rate of bursts originating at redshifts in the interval between z and $z + dz$. The rate is given by Eq. (59) of [31]

$$\frac{dR}{dz} = H_0 \frac{N_c (g_2 f_* H_0^{-1})^{-2/3}}{2\alpha^{5/3} p\Gamma G\mu} \varphi_t^{-14/3}(z)\varphi_V(z)(1 + z)^{-5/3}$$
$$\times \Theta(1 - \theta_m(z, f_*, \alpha H_0^{-1}\varphi_t(z)), \qquad (11)$$

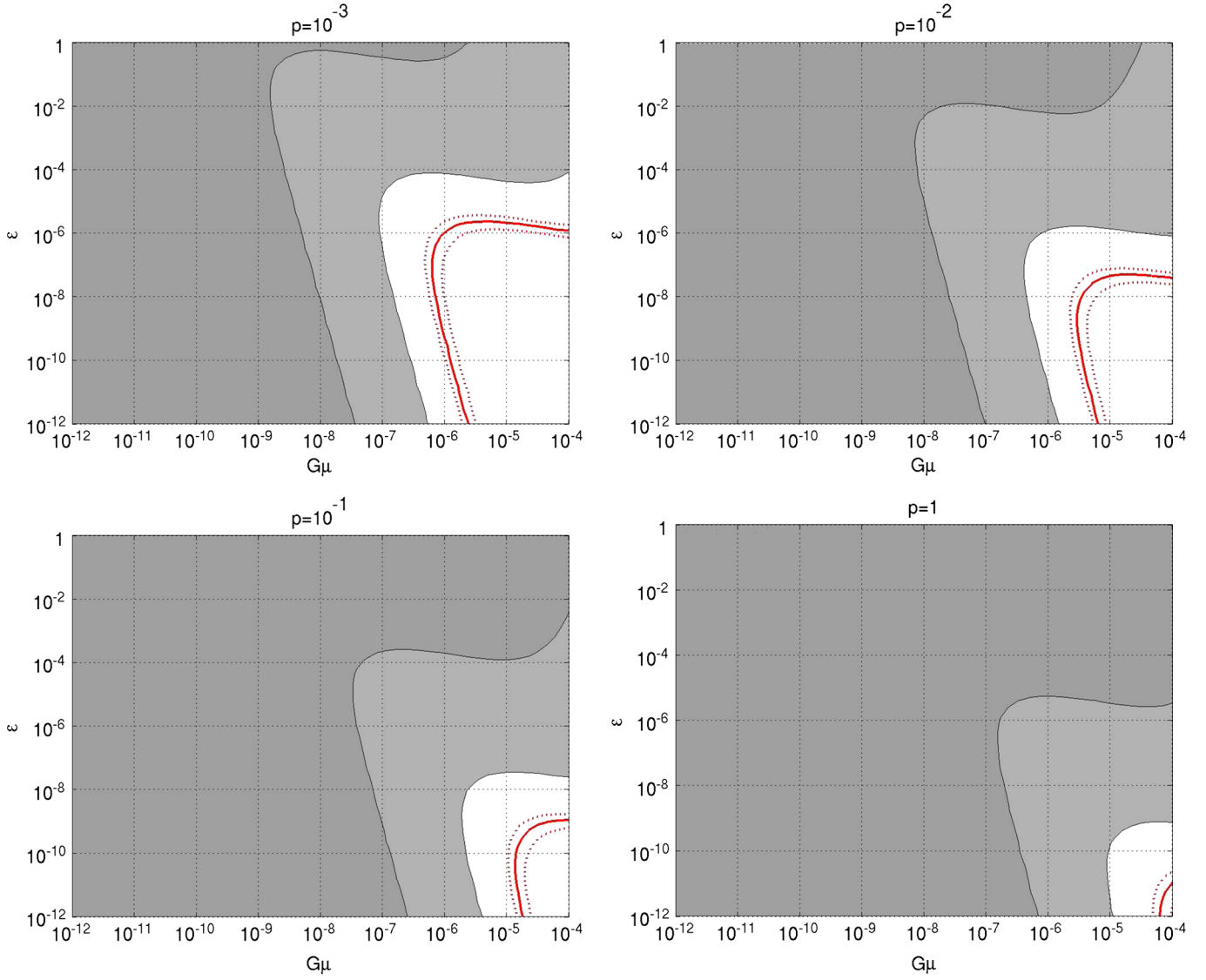where H_0 is the present value of the Hubble parameter; N_c

FIG. 3 (color online).   Plot of the sensitivity and upper limit results of our analysis. Each of the four panels corresponds to a value of the reconnection probability p with y axes ε and x axes $G\mu$. Areas to the right of the thick solid (red) curves show the regions excluded at the 90% level by our analysis. The dotted curves indicate the uncertainty in the areas of parameter space excluded that arise from uncertainties in the efficiency. The light and dark gray shaded areas are regions of parameter space unlikely to result in a cosmic string cusp event detected in S4: a cosmic string network with model parameters in these regions would result in less than one event (on average) surviving our pipeline. The lower boundary of these shaded areas was computed using the efficiency for all recovered injections, the dashed curve shown in Fig. 2. The dark gray regions show regions of parameter space unlikely to result in a cosmic string cusp being detected in a year long search of initial LIGO data. The lower boundary of the dark gray areas was computed with the initial LIGO sensitivity estimate $B_{50\%}^{\mathrm{LIGO}} \approx 10^{-20}\ \mathrm{s}^{-1/3}$ [31].

is the average number of cusps per loop oscillation; g_2 is an ignorance constant that absorbs the unknown fraction of the loop length that contributes to the cusp and other factors of $O(1)$; f_* is the lowest high frequency cutoff of the bursts we are interested in detecting; $\alpha = \varepsilon\Gamma G\mu$ is the loop formation size in units of the cosmic time; and $\theta_m = [g_2(1 + z)f_*l]^{-1/3}$ is the maximum angle a cusp and the line of sight can subtend and still produce a burst with high frequency cutoff f_*. The Θ function removes events that do not have the form of Eq. (1). Two dimensionless cos-

mological functions enter the expression for the rate of events: $\varphi_t(z)$ which relates the cosmic time t and the redshift via $t = H_0^{-1}\varphi_t(z)$, and $\varphi_V(z)$ which determines the proper volume element at a redshift z through $dV(z) = H_0^{-3}\varphi_V(z)dz$ (see Appendix A of [31]). For details on the derivation of this expression, see [28–31].

The efficiency $\epsilon(z)$ is the fraction of events we detect from a redshift z. We compute this quantity starting from our measured efficiency as a function of the amplitude B, using Eq. (60) of [31]

$$\frac{\varphi_t^{2/3}(z)}{(1+z)^{1/3}\varphi_r(z)} = \frac{BH_0^{-1/3}}{g_1 G\mu\alpha^{2/3}}, \qquad (12)$$

where g_1 is an ignorance constant that absorbs the unknown fraction of the loop length that contributes to the cusp and factors of $O(1)$ (different from those of g_2; see [31] for details), and $\varphi_r(z)$ is a dimensionless cosmological function that relates the proper distance r to the redshift via $r = H_0^{-1}\varphi_r(z)$. Solving Eq. (12) for z gives the redshift from which a burst of amplitude B originates. Thus for each amplitude in our efficiency curve, we can determine the corresponding redshift and construct $\epsilon(z)$.

We have computed the cosmological functions $\varphi_r(z)$, $\varphi_t(z)$, and $\varphi_V(z)$, as described in Appendix A of [31], using the latest consensus cosmological parameters measured by WMAP [46]. Specifically, we used a present day Hubble parameter of $H_0 = 70.1$ km s^{-1} Mpc^{-1} = 2.27×10^{-18} s^{-1}, and densities relative to the critical density $\Omega_m = 0.279$ for matter, $\Omega_r = 8.5 \times 10^{-5}$ for radiation, and $\Omega_\Lambda = 1 - \Omega_m - \Omega_r = 0.721$ for the cosmological constant.

We scan the parameter space of the small loop models by varying the reconnection probability p, the dimensionless string tension $G\mu$, and the size of loops parametrized by ε. To construct a 90% upper limit, we use the loudest event statistic [37]. For each point in cosmic string parameter space, we compute the effective rate γ using the solid black curve in Fig. 2 (recovered injections with amplitudes above our loudest event). We then compare this rate with $\gamma_{90\%} = 2.303/T$, the rate for which 90% of the time, we would have seen at least one event in a Poisson process if we observed for a time T. If for a point in parameter space the effective rate $\gamma(G\mu, \varepsilon, p)$ exceeds $\gamma_{90\%}$, then we say those parameters are ruled out at the 90% level, in the sense that cosmic string models with those parameters would have produced an event with an amplitude larger than our loudest event 90% of the time. We can also estimate our sensitivity by computing γ using the dashed curve in Fig. 2 (recovered injections with any amplitude) and then compare it to $1/T$. The latter tells us what models would have resulted in at least one event (on average) surviving our pipeline, a useful measure of our sensitivity. For our search in triple coincident S4 data, $T = 14.9$ days.

Figure 3 shows the results of our analysis. We have set $N_c = g_1 = g_2 = 1$ for convenience. Each of the four panels corresponds to a value of the reconnection probability p with the loop size parameter ε on the y axis, and the dimensionless string tension $G\mu$ on the x axis. Regions to the right of the red curves are excluded at the 90% level by our analysis. The dotted curves show the uncertainty in the areas of parameter space excluded that result from uncertainties in the efficiency. The light and dark gray shaded areas in each of the four panels are regions of parameter space very unlikely to result in a cosmic string

cusp event detected in S4: a cosmic string network with model parameters in these regions would result in less than one event (on average) surviving our pipeline. The lower boundary of these areas was computed using the efficiency for all injections, the dashed curve shown in Fig. 2, and comparing the effective rate to $1/T$. The dark gray regions show regions of cosmic string model parameter space unlikely to result in a cosmic string cusp being detected in a year long search of initial LIGO data: on average, such models would result in fewer than one event being detected. The lower boundary curve of the dark gray regions was computed with the initial LIGO sensitivity estimate $B_{50\%}^{\text{LIGO}} \approx 10^{-20}$ s$^{-1/3}$ [31] and assuming a year of observation time.

Because of the sensitivity and duration of the S4 run, the 90% limits we have placed on the parameter space of cosmic string models are not as constraining as the indirect bounds due to big bang nucleosynthesis [38]. Another current gravitational wave bound comes from pulsar timing observations. Because of their sensitivity at very low frequencies, pulsar timing bounds for loop sizes given by gravitational back reaction constrain an independent portion of the cosmic string parameter space [38]. Future analysis of data from the fifth science run, however, a factor of 2 more sensitive and with a year of triple coincident data, will be sufficiently sensitive to surpass these limits in large areas of cosmic string parameter space.

VI. SUMMARY

We have performed a search for bursts from cosmic string cusps in 14.9 days of triple coincident data from LIGO's fourth science run. The gravitational waveforms of cosmic string cusps are known, and matched filters provide the optimal means of extracting such signals from noisy data. We constructed a template bank and generated a set of triggers for each of the three LIGO interferometers. To reduce the rate of accidentals, we demanded the resulting triggers satisfy two consistency criteria: (i) time coincidence between events in the three instruments, and (ii) amplitude consistency between events in the two Hanford interferometers H1 and H2. The latter check is possible, because the Hanford instruments are coaligned. The effect of the consistency criteria is to reduce the trigger rate in each of the instruments from about 1 Hz to about 10 μHz. To estimate our background, the rate of accidentals, we performed 100 time slides on the data, with a time step much larger than the duration of our signals. Comparing our background estimate with our foreground, we conclude no gravitational waves have been found in this search.

To estimate the sensitivity of the search and place constraints on the parameter space of cosmic strings, we performed several thousand simulated signal injections into our data streams and attempted to recover them. The

simulated signal parameters used are consistent with our expectations for the cosmic string population. The injections were used to compute the efficiency, the fraction of events that we detect in a range of amplitudes. The efficiency curves can be convolved with the cosmological rate of events to compute the so-called effective rate: the rate of detectable events in our search. The effective rate folds together the properties of the population, such as the distribution of sources in the sky, with the sensitivity of the detectors and the analysis pipeline. We found our estimate for the sensitivity of this search to be consistent with our expectations, given that we used S4 data and included H2 in the analysis. Using the loudest event in our foreground, we placed a frequentist 90% upper limit on the effective rate, which we in turn used to constrain the parameter space of cosmic strings models. Unfortunately, the sensitivity of this search does not allow us to place constraints as tight as the indirect bounds from big bang nucleosynthesis. However, analyses using data from future LIGO runs are expected to surpass these limits for large areas of cosmic string parameter space.

[1] T. W. B. Kibble, J. Phys. A **9**, 1387 (1976).

[2] A. Vilenkin and E. Shellard, *Cosmic Strings and other Topological Defects* (Cambridge University Press, Cambridge, United Kingdom, 2000).

[3] R. Jeannerot, J. Rocher, and M. Sakellariadou, Phys. Rev. D **68**, 103514 (2003).

[4] N. T. Jones, H. Stoica, and S. H. H. Tye, J. High Energy Phys. 07 (2002) 051.

[5] S. Sarangi and S. H. H. Tye, Phys. Lett. B **536**, 185 (2002).

[6] G. Dvali and A. Vilenkin, J. Cosmol. Astropart. Phys. 03 (2004) 010.

[7] N. T. Jones, H. Stoica, and S. H. H. Tye, Phys. Lett. B **563**, 6 (2003).

[8] E. J. Copeland, R. C. Myers, and J. Polchinski, J. High Energy Phys. 06 (2004) 013.

[9] M. G. Jackson, N. T. Jones, and J. Polchinski, J. High Energy Phys. 10 (2005) 013.

[10] S. H. H. Tye, I. Wasserman, and M. Wyman, Phys. Rev. D **71**, 103508 (2005).

[11] E. J. Copeland, T. W. B. Kibble, and D. A. Steer, Phys. Rev. D **75**, 065024 (2007).

[12] L. Leblond and M. Wyman, Phys. Rev. D **75**, 123522 (2007).

[13] A. Rajantie, M. Sakellariadou, and H. Stoica, J. Cosmol. Astropart. Phys. 11 (2007) 021.

[14] P. Bhattacharjee and G. Sigl, Phys. Rep. **327**, 109 (2000).

[15] V. Berezinsky, B. Hnatyk, and A. Vilenkin, Phys. Rev. D **64**, 043004 (2001).

[16] D. Battefeld, T. Battefeld, D. H. Wesley, and M. Wyman, J. Cosmol. Astropart. Phys. 02 (2008) 001.

[17] D. F. Chernoff and S. H. H. Tye, arXiv:0709.1139.

[18] K. Kuijken, X. Siemens, and T. Vachaspati, Mon. Not. R. Astron. Soc. **384**, 161 (2008).

[19] M. A. Gasparini, P. Marshall, T. Treu, E. Morganson, and F. Dubath, arXiv:0710.5544.

[20] J. L. Christiansen, E. Albin, K. A. James, J. Goldman, D. Maruyama, and G. F. Smoot, Phys. Rev. D **77**, 123509 (2008).

[21] S. Dyda and R. H. Brandenberger, arXiv:0710.1903.

[22] T. Vachaspati, Phys. Rev. Lett. **101**, 141301 (2008).

[23] R. Khatri and B. D. Wandelt, Phys. Rev. Lett. **100**, 091302 (2008).

[24] A. A. Fraisse, C. Ringeval, D. N. Spergel, and F. R. Bouchet, Phys. Rev. D **78**, 043535 (2008).

[25] L. Pogosian, S. H. Tye, I. Wasserman, and M. Wyman, J. Cosmol. Astropart. Phys. 02 (2009) 013.

[26] D. Baumann *et al.*, arXiv:0811.3911.

[27] V. Berezinsky *et al.*, arXiv:astro-ph/0001213.

[28] T. Damour and A. Vilenkin, Phys. Rev. Lett. **85**, 3761 (2000).

[29] T. Damour and A. Vilenkin, Phys. Rev. D **64**, 064008 (2001).

[30] T. Damour and A. Vilenkin, Phys. Rev. D **71**, 063510 (2005).

[31] X. Siemens *et al.*, Phys. Rev D **73**, 105001 (2006).

[32] X. Siemens and K. D. Olum, Phys. Rev. D **68**, 085017 (2003).

[33] D. Chialva and T. Damour, J. Cosmol. Astropart. Phys. 08 (2006) 003.

[34] A. Abramovici *et al.*, Science **256**, 325 (1992); B. Barish and R. Weiss, Phys. Today **52**, 44 (1999).

[35] B. Caron *et al.*, Nucl. Phys. B, Proc. Suppl. **54**, 167

(1997).

[36] D. Sigg (LIGO Scientific Collaboration), Classical Quantum Gravity **23**, S51 (2006).

[37] P. R. Brady *et al.*, Classical Quantum Gravity **21**, S1775 (2004).

[38] X. Siemens, V. Mandic, and J. Creighton, Phys. Rev. Lett. **98**, 111101 (2007).

[39] X. Siemens *et al.*, Classical Quantum Gravity **21**, S1723 (2004).

[40] C. Cutler and E. E. Flanagan, Phys. Rev. D **49**, 2658 (1994).

[41] B. Allen, W. G. Anderson, P. R. Brady, D. A. Brown, and

J. D. E. Creighton, arXiv:gr-qc/0509116.

[42] X. Siemens, K. D. Olum, and A. Vilenkin, Phys. Rev. D **66**, 043501 (2002).

[43] J. Polchinski and J. V. Rocha, Phys. Rev. D **75**, 123503 (2007).

[44] V. Vanchurin, K. D. Olum, and A. Vilenkin, Phys. Rev. D **74**, 063527 (2006).

[45] K. D. Olum and V. Vanchurin, Phys. Rev. D **75**, 063521 (2007).

[46] http://lambda.gsfc.nasa.gov/product/map/dr3/parameters_summary.cfm.